



Article

Zn²⁺-Doped TiO₂:WO₃ Films Prepared by Electrospinning and Sintering: Microstructural Characterization and Electrical Signature to Moisture Sensing

Georges M. G. Silva ^{1,2}, Victor N. S. Leão ¹, Michel F. G. Pereira ¹, Pedro M. Faia ³  and Evando S. Araújo ^{1,*} 

- ¹ Research Group on Electrospinning and Nanotechnology Applications, Department of Materials Science, Federal University of San Francisco Valley, Juazeiro 48902-300, Brazil; georges.gil@ifsertao-pe.edu.br (G.M.G.S.); victornleao@gmail.com (V.N.S.L.); michelgalvao2014@gmail.com (M.F.G.P.)
- ² Federal Institute of Education, Science and Technology of the Sertão Pernambucano, Petrolina 56314-520, Brazil
- ³ CEMMPRE—Electrical and Computer Engineering Department, FCTUC, University of Coimbra, Polo 2, Pinhal de Marrocos, 3030-290 Coimbra, Portugal; faia@deec.uc.pt
- * Correspondence: evando.araujo@univasf.edu.br; Tel.: +55-74-2102-7645

Abstract: In this work, Zn²⁺-doped TiO₂:WO₃ nanostructured films, with different doping levels, were produced by electrospinning followed by sintering, and tested as potential materials for relative humidity (RH) detection. The materials microstructure was investigated by scanning electron microscopy (SEM), energy dispersive spectroscopy (EDS), Fourier-transform infrared spectroscopy (FTIR), Raman spectroscopy, and X-ray diffraction (XRD). The electrical characterization was performed by electrical impedance spectroscopy in the range of 400 Hz–40 MHz, at 20 °C. The sensors' sensitivity to moisture was evaluated from the impedance variations in response to changes in RH (10–100%). The analyses confirmed the interaction of water molecules with the oxides surface, and showed that zinc atoms were incorporated into the titanium vacancies in the crystal lattice. All the studied sensors showed a p- to n-type conduction transition taking place at around 40% RH. The nanocomposite with 2 wt% of dopant presented the best sensitivity to moisture, with an impedance variation of about 1 order of magnitude. The results are discussed in relation to the microstructure and fabrication route.



Citation: Silva, G.M.G.; Leão, V.N.S.; Pereira, M.F.G.; Faia, P.M.; Araújo, E.S. Zn²⁺-Doped TiO₂:WO₃ Films Prepared by Electrospinning and Sintering: Microstructural Characterization and Electrical Signature to Moisture Sensing. *Ceramics* **2021**, *4*, 576–591. <https://doi.org/10.3390/ceramics4040041>

Academic Editors: Giuseppe Viola and Gilbert Fantozzi

Received: 31 July 2021

Accepted: 14 October 2021

Published: 21 October 2021

Publisher's Note: MDPI stays neutral with regard to jurisdictional claims in published maps and institutional affiliations.



Copyright: © 2021 by the authors. Licensee MDPI, Basel, Switzerland. This article is an open access article distributed under the terms and conditions of the Creative Commons Attribution (CC BY) license (<https://creativecommons.org/licenses/by/4.0/>).

Keywords: humidity sensing; electrospinning; metal oxide heterogeneous nanostructures; microstructural characterization; electrical properties

1. Introduction

Relative humidity (RH) is one of the most important environmental parameters for prevention and monitoring of a wide variety of processes in medical, food and industrial sectors [1].

Moisture sensors are the most commonly used instruments in monitoring this parameter. Several materials have been tested and used for this application, such as conductive polymers [2], carbon-based materials [3], metal oxides [4], and their composites [5], based on the notable variation in their electrical response as a function of RH.

Metal oxide-based moisture sensors have received attention due their excellent combined properties such as flexibility, chemical and structural stability, electroactivity, reproducibility and possibility of applications over a wide range of relative humidity [4,6]. More recently, titanium (IV) oxide (TiO₂)-based metal oxide heterogeneous nanostructures (MOHN) have been receiving increasing interest, and have been studied as potential materials for the development of high sensitivity and low cost moisture sensing devices [7].

In this configuration, the interaction at the atomic and surface level between TiO₂ and the other oxide constituents enables the improvement of the electrical and struc-

tural properties of the resulting material (when compared to the use of pure TiO₂) and, consequently, the moisture sensing [7]. The choice of selective oxides, dopant ions and fabrication route are other factors that directly influence the obtention of sensors with high surface area/volume ratio, and consequently higher sensitivity to RH [8]. In this sense, Zanetti et al. [9] showed that the addition of tungsten (VI) oxide (WO₃) to TiO₂ by sintering improves the stability of the TiO₂ anatase phase and the sensitivity to relative humidity, due to the occurrence of surface heterojunction between the oxides. The results still revealed decreasing pore size and smaller variance in particle size distribution, which improves the chemisorption of water molecules on the semiconductors surface.

In the fabrication procedure of these sensing materials, in the form of volumetric pellets, the mechanical alloying method was introduced before the usual molding and sintering steps [10]. The results showed that the change in the preparation route was the main reason for obtaining heterogeneous nanostructures with smaller particle size, larger surface area, greater stability to phase transitions, changes in electrical behavior at low RH and improved sensitivity.

More recently, Araújo and Leão [11] indicated that it is possible to produce heterogeneous TiO₂:WO₃ nanostructures with high moisture sensitivity, using an alternative preparation route that combines electrospinning and sintering. In these systems, the surface area/volume ratio was higher than that observed for the TiO₂:WO₃ pelletized systems [10,12], while the amount of material by about three orders of magnitude [11] could lead to the miniaturization of sensor devices.

Based on previous studies on moisture sensors produced from TiO₂ and WO₃ heterogeneous nanostructures doped with diverse selective ions (V⁵⁺, Nb⁴⁺, Zn²⁺, In³⁺, among others) [9,10,12,13], using various fabrication routes [10,13], this work investigates the electrical signature to moisture of Zn²⁺-doped TiO₂:WO₃ MOHN films produced by electrospinning followed by sintering.

The selection of zinc as a dopant was based on previous reports [12,14–17], which evidenced that the use of zinc could increase the sensitivity of the composite sensors.

All the obtained sensors showed a p- to n-type conduction transition taking place at around 40% RH, different from what was observed with pelletized samples of the same compositions previously tested, which exhibited n-type conduction along the full RH range [13].

The conduction mechanisms and electrical response of the samples to RH variations were directly related to the alternative fabrication process and the resulting microstructure of the final materials.

2. Materials and Methods

2.1. Materials

Methacrylic acid-methyl methacrylate copolymer (Evonik), ethanol PA (99.8 %, Neon Comercial, Suzano, Brazil), titanium (IV) oxide (anatase TiO₂, <25 nm particle size, 99.7% trace metals basis, Sigma Aldrich, Burlington, VT, USA), tungsten (VI) oxide (WO₃, <100 nm particle size, Sigma Aldrich) and zinc oxide (ZnO, <50 nm particle size, >97%, Sigma Aldrich) chemicals were used as raw materials.

2.2. Sample Preparation

In brief, the samples for the humidity sensitivity tests were prepared by electrospinning of the metal oxide-containing copolymer solution, followed by the sintering process of the electrospun composite fibers [9].

The polymer solutions for the electrospinning procedure were prepared from 1.6 g of copolymer diluted in 6.0 mL of ethanol.

The metal oxide heterogeneous nanostructures (MOHN samples) were defined as: TW (TiO₂:WO₃ base mixture, with 48.9:51.1 wt% proportion of these oxides, respectively); TW – Zn2 and TW – Zn4 (98:2 and 96:4 weight ratio of the TW mixture and ZnO, respectively).

Then, 4 mL of polymer solution containing 0.50 g of each *MOHN* sample were introduced into a syringe (10 mL capacity and 0.7 mm metallic capillary diameter) and injected under constant pressure, with a flow rate of $100 \mu\text{L min}^{-1}$ at the capillary tip (needle). An electric potential difference of 15 kV was applied between the needle and a grounded plane metal collector ($10 \times 10 \text{ cm}^2$), separated by a distance of 10 cm, to allow the electrospun polymer/*MOHN* fibers production on the collector surface. The collected fibers were then deposited over a pair of gold (*Au*) interdigitated electrodes ($1.1 \text{ cm} \times 1.1 \text{ cm}$), previously printed on an alumina substrate. All experiments were carried out at $20 \text{ }^\circ\text{C}$.

Each sample on the substrates was then sintered in an oven at $500 \text{ }^\circ\text{C}$ for 2 h, in order to obtain the final *MOHN* films for electrical characterization. The choice of the just mentioned sintering conditions was based on previous studies [13,15], which showed favourable moisture behaviour under similar sintering conditions. Figure 1 illustrates the procedure for the preparation of *MOHN* and the characterization of the humidity sensing properties.

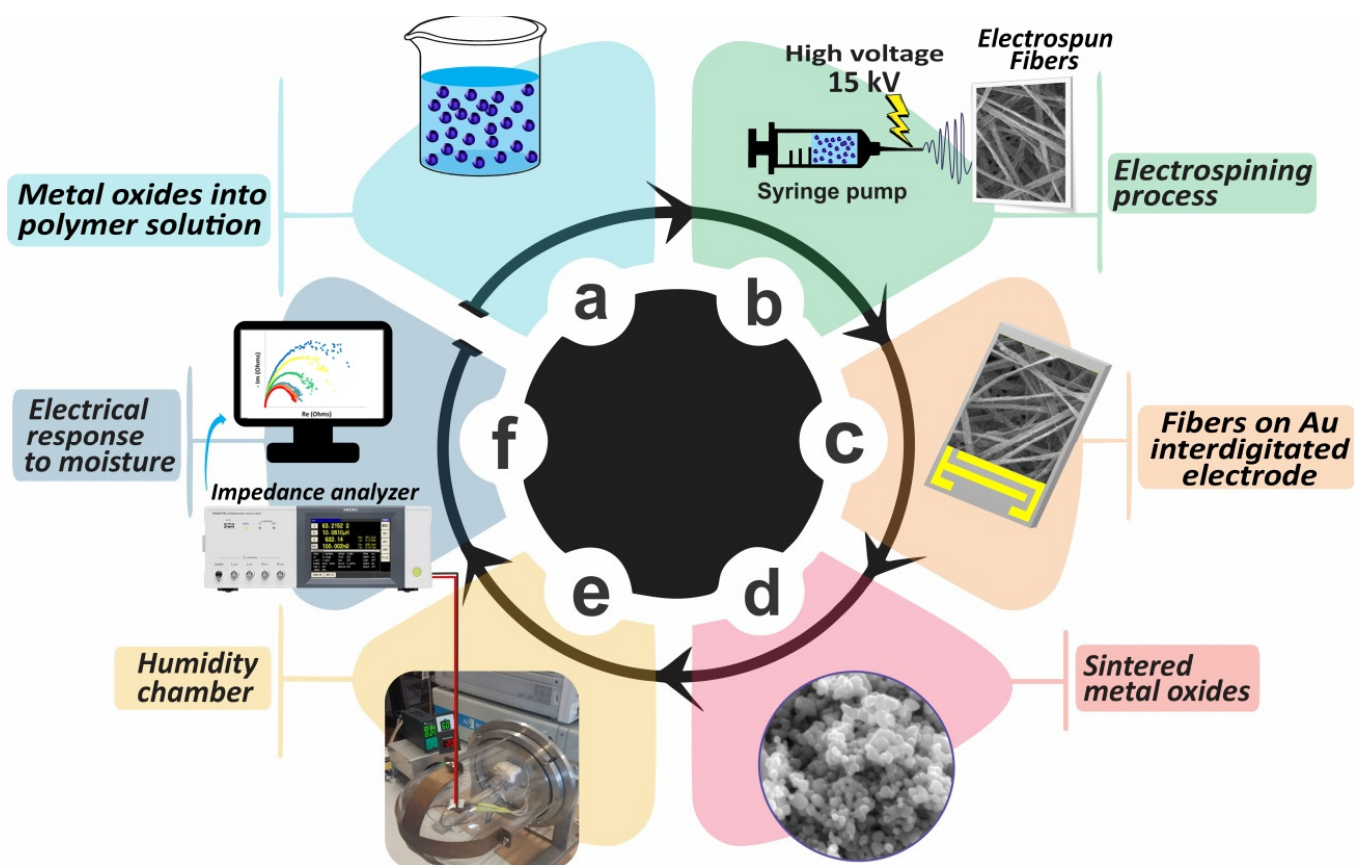


Figure 1. Schematic illustration of the sensor materials production and electrical response testing to RH. (a) Metal oxides into polymer solution; (b) electrospinning process; (c) fibers on electrodes; (d) sintered metal oxides; (e) humidity chamber used for electrical characterization; (f) impedance spectroscopy.

2.3. Microstructural Characterization

The materials microstructure was investigated by scanning electron microscopy (SEM) and energy dispersive spectrometry (EDS), by which elemental composition mappings were generated, using a Vega 3XM Tescan equipment (Tescan, Brno, Czech Republic), 10 to 20 kV accelerating voltage. Fourier Transform Infrared spectroscopy (FTIR) was carried out in transmission mode in the wavenumber range from 400 to 4000 cm^{-1} , using *KBr* pellets (Schimadzu Prestige 21 equipment, Shimadzu Corporation, Kyoto, Japan). Raman spectra were obtained using 532 nm laser wavelength, 20–25 mW (HORIBA Scientific, Osaka,

Japan). X-ray diffraction (XRD) patterns in the range 15–70° with a scan rate of 0.02°s⁻¹, were generated using a Miniflex Rigaku equipment (Rigaku Corporation, Tokyo, Japan), Cu K α radiation ($\lambda_{Cu} = 1.5406 \text{ \AA}$), 15 mA current and 40 kV voltage. The crystalline phases were identified using X-Pert HighScore software, while the crystallographic data were obtained from the International Center for Diffraction Data (ICDD).

2.4. Electrical Response

The obtained *MOHN* samples' electrical response dependence with relative humidity, RH, was investigated by electrical impedance spectroscopy (impedance analyzer HP4194A, Hewlett-Packard, Santa Clara, CA, USA), in the frequency range from 400 Hz to 40 MHz. The samples were placed inside a test chamber with a volume of approximately 6.5 L, at a temperature of 20 °C, in which moisture concentration and temperature were automatically controlled, with an error smaller than $\pm 1\%$. RH values ranging from 10 to 100%, were obtained by mixing dry air and fully humidified air in the desired proportions. The sensitivity of the samples to RH changes was evaluated using calculated impedance module values, $|Z|$ ($|Z| = \sqrt{(Z')^2 + (Z'')^2}$), where Z' and Z'' are the resistance and the reactance of the measured impedance by impedance spectroscopy. All depicted electrical results, are the medium values calculated for each frequency of two sets of sweep measures taken in two different moments in time.

2.5. Statistical Analysis

The analyses of fiber diameter and crystallite and particle size of the sintered structures were given as the average of three independent measurements, for each *MOHN* configuration. Normality and equality of means tests were performed with significance level, α , of 0.05 and compared to the p -value returned by statistical tests. Sample sizes (n) were obtained from SEM images using ImageJ software.

3. Results and Discussion

3.1. Microstructural Analysis

The SEM micrographs and EDS mappings of the *TW – Zn2* and *TW – Zn4 MOHN*-loaded fibers are shown in Figure 2. The surface morphology analysis returned regular diameter composite fibers with no apparent structural defects, indicating that the electrospinning process parameters were adequate for preparation of these materials (first step of sensors production).

The mean diameters of *TW*, *TW – Zn2* and *TW – Zn4* fibers were estimated as $6.4 \pm 1.7 \text{ \mu m}$ ($n = 59$) [11], $6.4 \pm 1.5 \text{ \mu m}$ ($n = 69$) and $6.7 \pm 2.3 \text{ \mu m}$ ($n = 62$), respectively. All *MOHN*-loaded fiber configurations presented diameters with normal distribution. In addition, the hypothesis tests on the population mean difference, with unknown standard deviation, revealed that there is no statistically significant difference in the mean diameter of the composite fibers (p -value $> \alpha$).

The EDS elemental composition and maps of the *MOHN* models-loaded fibers confirmed that the Ti, W, Zn and O element populations are evenly distributed in the polymer matrix, as exemplified for the *TW – Zn2* sample (Figure 2c). In addition, these combined analyses indicate that the moisture sensitivity of the nanocomposites is mainly influenced by the microstructure of the oxides and their interactions, since there is no significant variation in the volume fraction of nanoparticles in the produced polymeric matrices.

With electrospinning, particle aggregation is minimized and dispersion of the *MOHN* combinations over the interdigitated electrodes is promoted. As a consequence, higher surface contact areas, and in turn, with higher sensitivity materials to RH are expected [11]. In other words, electrospinning proves to be a simple and low-cost technique (when compared with other methods such as coating and sputtering [18]) that can be viably used for the deposition of metal oxides on substrates.

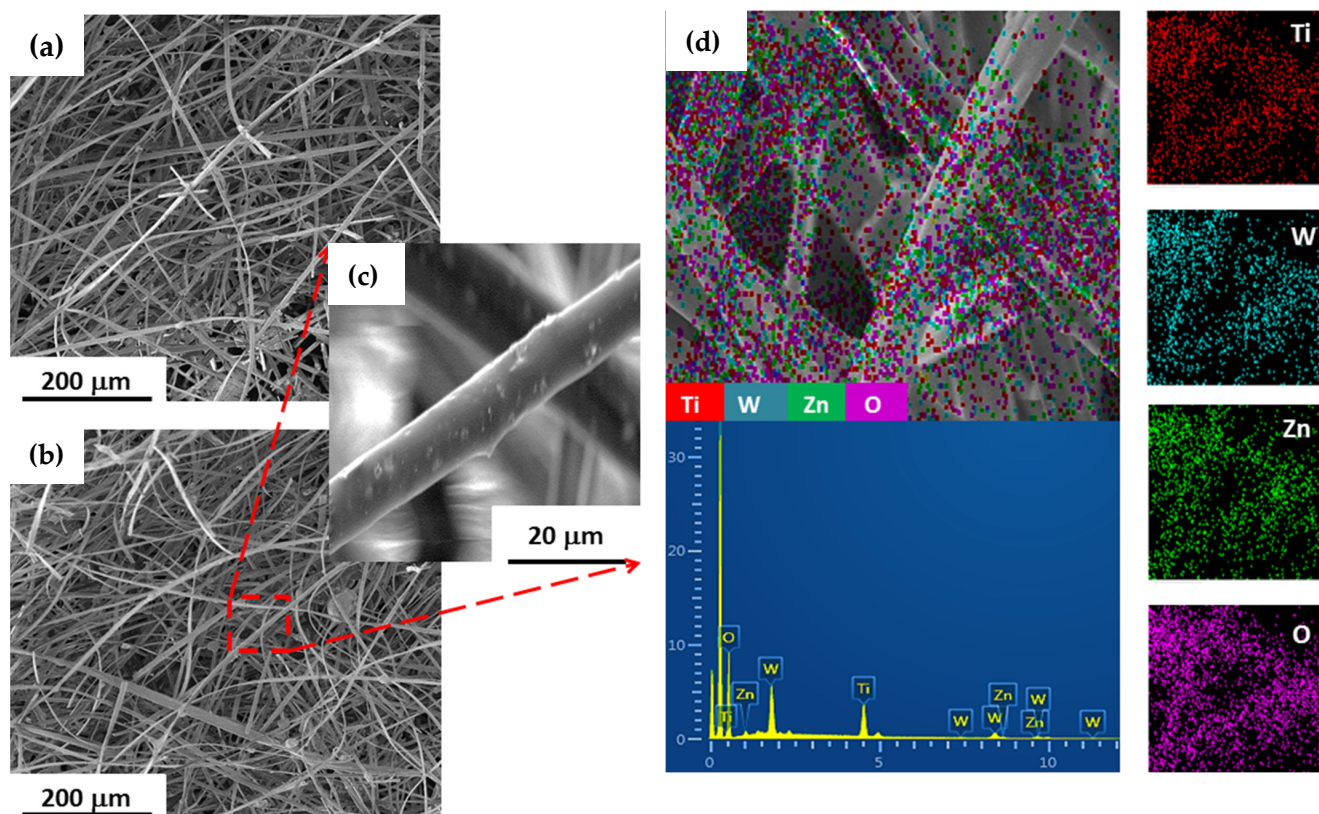


Figure 2. Scanning electron microscopy (SEM) images of *TW – Zn MOHN*-loaded electrospun fibers with (a) 2 wt% and (b) 4 wt% of zinc oxide (ZnO); (c) representative SEM micrograph of the fiber surface and (d) energy dispersive spectroscopy (EDS) elemental composition and mapping of *TW – Zn2* samples.

Thus, it is possible to produce sensing materials with a high surface area to volume ratio, which directly leads to better RH sensitivity. The application of *MOHN* as RH sensors involves the processes of chemisorption and physisorption of water molecules on the oxides surface. Additionally, the improved efficiency of these processes is also directly related with the larger porosity of sensing materials, as expected for the case of *MOHN* produced by electrospinning [11].

The surface morphology of the materials used for the electrical response tests to moisture, resulting from the sintering process at 500 °C, is shown in Figure 3. After sintering, the obtained initial fibrous morphology is no longer present, however, based on the SEM images, the obtained nanostructures seem to present significant overall contact surface together with open porosity.

The EDS analyses of the sintered *MOHN* confirmed the continuity of the uniform distribution of Ti:W metal matrix and of the zinc dopant, as shown for the *TW – Zn2* sample (Figure 3c). The micrographs of *TW – Zn2* and *TW – Zn4* samples revealed a porous nanostructure, with spherical particles in the order of 100–250 nm, and free of polymeric phase. These features are known to favor the application of these structures for RH sensing, as discussed earlier. The mean sample diameters were calculated to be 145.7 ± 47.0 nm ($n = 135$) [11], 165.1 ± 64.1 nm ($n = 115$) and 179.7 ± 73.5 nm ($n = 122$), for *TW*, *TW – Zn2* and *TW – Zn4* systems, respectively.

The hypothesis tests' analyses for the difference in mean particle diameter showed that there were no significant differences in particle size among the all produced sintered *MOHN* (p -value > α , for all mean comparisons). This proves that the best results for the sensitivity of these systems to RH are predominantly related to the atomic and surface interaction levels between the constituent oxides of the nanocomposites. It is important to, once more, point out that all morphological characteristics discussed here (such as nanometric size, spherical shape, porosity and regular distribution) are fundamental for

RH sensing, since they favor the adsorption processes of water vapor from the environment, on the oxides surface and the porous structure.

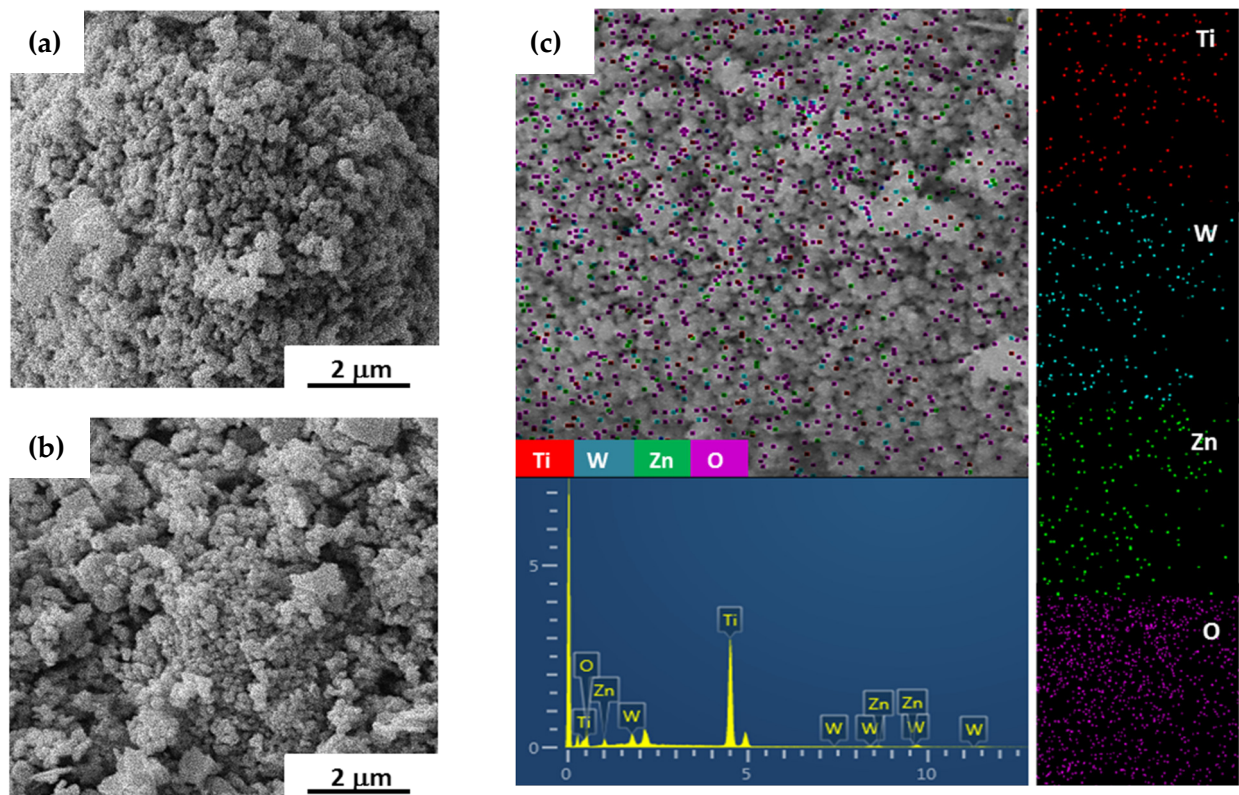


Figure 3. SEM micrographs of (a) $TW - Zn_2$ and (b) $TW - Zn_4$ MOHN after the sintering process; and (c) EDS elemental composition and mapping of sintered $TW - Zn$ samples, with indication of titanium (Ti), tungsten (W), zinc (Zn), and oxygen (O) elements.

The FTIR spectra of the polymer matrix and sintered samples are shown in Figure 4a. For all three MOHN samples, it is possible to observe a broad transmission band in the $470\text{--}1000\text{ cm}^{-1}$ wavenumber range, due to the superposition of bands belonging to the different metal oxides present in the structures. In addition, the characteristic bands of the polymer matrix in the range of $1000\text{ to }3600\text{ cm}^{-1}$ (including the broad band around 3380 cm^{-1} due to the adsorbed water molecules by the polymer) [19], are not observed in the MOHN spectra, proving that the sensor materials are free from the organic phase, as suggested by the results obtained by SEM.

The X-ray diffractograms of the TW , $TW - Zn_2$, and $TW - Zn_4$ MOHN are presented in Figure 4b. The characteristic crystallographic planes of the anatase TiO_2 with tetragonal structure ($a = b = 3.7821\text{ \AA}$ and $c = 9.5022\text{ \AA}$ lattice constants [20]) and monoclinic WO_3 ($a = 7.306\text{ \AA}$, $b = 7.540\text{ \AA}$ and $c = 7.692\text{ \AA}$ [21]) were confirmed in the experimental data of the three composite systems, from 01-071-1166 and 01-083-0951 ICDD cards, respectively. The results show that the electrospinning and sintering processes at $500\text{ }^\circ\text{C}$ causes no phase change or solid solution formation from these oxides in the tested MOHN [1,22].

In all three samples, the experimental values of WO_3 unit cell parameters ($a = 7.31\text{ \AA}$, $b = 7.54\text{ \AA}$, $c = 7.69\text{ \AA}$, $\alpha = \gamma = 90^\circ$ and $\beta = 90.88^\circ$) showed no significant changes, related to pristine oxide. The lattice parameters for TiO_2 in the TW sample were calculated to be $a = b = 3.78\text{ \AA}$ and $c = 9.51\text{ \AA}$, $\alpha = \beta = \gamma = 90^\circ$ [11], in accordance with the data of the starting material. In addition, it is possible to verify in Table 1 the dependence of TiO_2 parameters on Zn concentrations in the $TW - Zn_2$ and $TW - Zn_4$ samples. A decrease in the values of a and b parameters, and an increase in the value of c , from the undoped

material to the doped material with 2 wt% of zinc, can be noticed, due to a variation in the volume of the TiO_2 unit cell. The $TW - \text{Zn}4$ sample, on the other hand, does not present significant changes in the values of these parameters (no change in the cell volume), compared to the $TW - \text{Zn}2$ sample, indicating that part of the zinc concentration remains on the surface material after the interaction saturation between zinc and titanium ions at the atomic level.

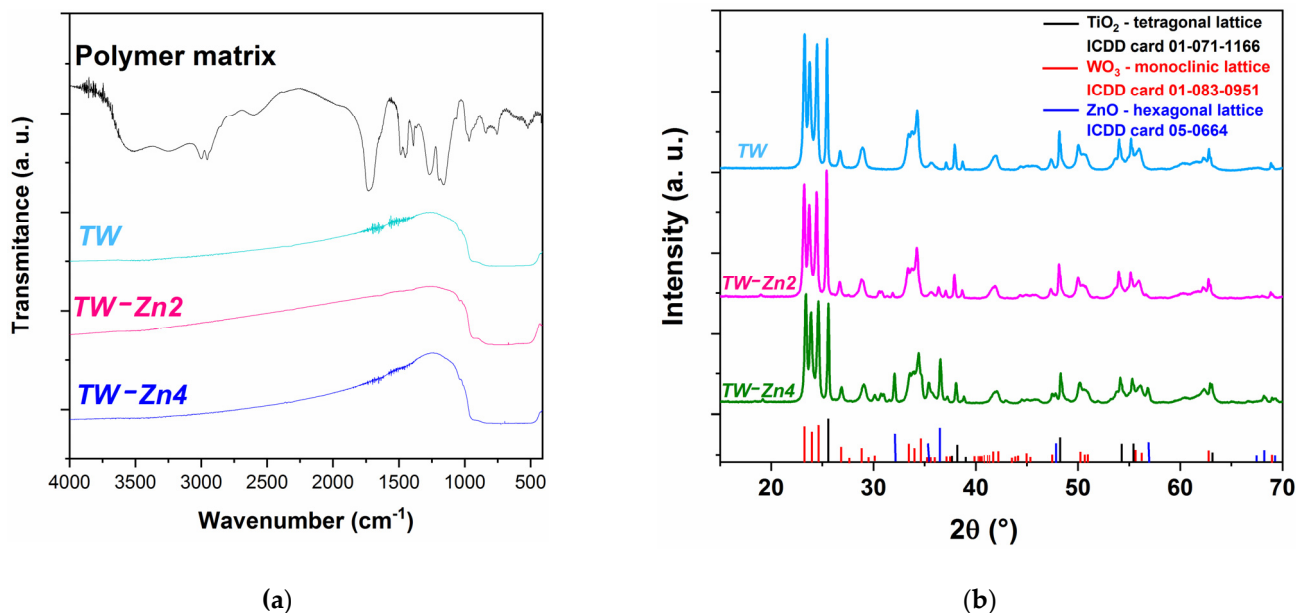


Figure 4. (a) FTIR spectra and (b) X-ray diffractograms of the TW , $TW - \text{Zn}2$, and $TW - \text{Zn}4$ MOHN.

Table 1. Lattice parameters and crystallite size of TiO_2 in TW , $TW - \text{Zn}2$ and $TW - \text{Zn}4$ MOHN.

MOHN	Lattice Parameters (Å)		Average Crystallite Size, D (nm)
	a = b	C	
TW	3.78	9.51	19.12 (± 1.12)
$TW - \text{Zn}2$	3.69	9.73	24.27 (± 2.03)
$TW - \text{Zn}4$	3.70	9.70	23.75 (± 2.33)

In fact, there is the occurrence of zinc ion doping in the atomic structure of titanium: the ionic radius of Zn^{2+} ions (0.74 Å [23]) is close to that of Ti^{4+} ions, promoting the occupation of vacancies of the Ti atom sites by Zn elements, after the sintering process.

The crystallite average size (D) of the anatase TiO_2 (Table 1) and monoclinic WO_3 in the investigated TW , $TW - \text{Zn}2$ and $TW - \text{Zn}4$ nanocomposites was determined by the modified Scherrer equation (MSE), $D = \lambda/3\beta \cos(\theta)$ [24], where $1/3$ is the correction value of the shape factor K in Scherrer Equation [25]; λ is the X-ray radiation wavelength; β and θ are the full width half maxima and the half of the diffraction angle (2θ) at the crystal planes detected in the XRD spectrum, respectively.

The average size (D) of the WO_3 crystallites was estimated to be 15.01 (± 0.75) nm, 15.32 (± 1.22) nm and 15.95 (± 1.49) nm for TW , $TW - \text{Zn}2$, and $TW - \text{Zn}4$ samples, respectively. For TiO_2 , D values were calculated to be 19.12 (± 1.12) nm, 24.27 (± 2.03) nm, and 23.75 (± 2.33) nm, with increasing zinc concentration.

The equality of means test (with sample size $n = 3$ and level of significance $\alpha = 0.05$) showed that the WO_3 crystallite average sizes present no significant differences in the three tested systems. On the other hand, TiO_2 average size values calculated for the $TW - \text{Zn}2$ and $TW - \text{Zn}4$ compositions are significantly higher than that observed for the TW model. The D values in $TW - \text{Zn}2$ and $TW - \text{Zn}4$ samples did not show significant difference. These results corroborate the previously reported effects of dopant and indicate that ZnO at

4 wt% promotes saturation of the Zn/Ti atomic interactions, which increases the presence of surface interactions between the oxides. This behavior is confirmed by the emergence of ZnO peaks with a hexagonal crystal structure (from the (100) plane at $2\theta = 32.2^\circ$, and according to the supplier) in the diffractograms of doped samples.

The Raman spectra of the sintered *MOHN* are presented in Figure 5. The spectrum of pristine anatase TiO_2 sintered at 500°C was also analyzed for comparison with the *MOHN* spectra. The characteristic molecular vibration bands of the anatase phase were observed at 141, 195, 396, 515 and 637 cm^{-1} wavenumbers [26].

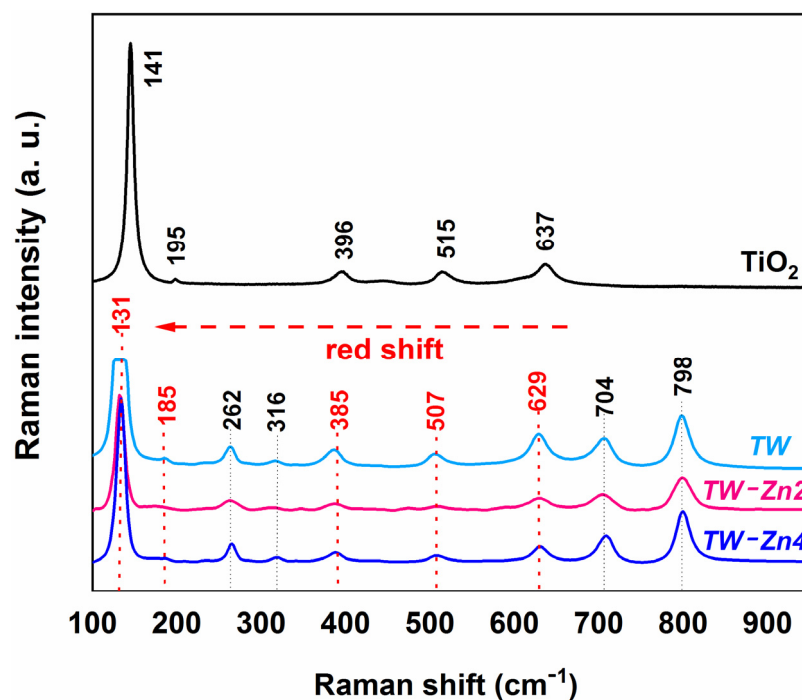


Figure 5. Raman spectra of anatase TiO_2 , *TW* and *TW - Zn* sintered *MOHN* (varying dopant concentrations).

These bands were also found in the *TW* and *TW - Zn* samples with 2 and 4 wt% of Zinc, but shifted to lower wavenumber regions (about $8\text{--}11\text{ cm}^{-1}$ shift) of the spectrum (red shift). In addition, the spectral analysis of undoped and Zn-doped samples proved the continuity of the WO_3 monoclinic structure after sintering at 500°C , with characteristic vibration bands at 262, 316, 704, and 798 cm^{-1} wavenumbers, as described in the literature [27,28].

The red shift phenomenon of TiO_2 vibrational bands is attributed to distortions and confinement of phonons in its crystalline lattice, promoted by the introduction of impurities in the atomic structure of the material [29]. In fact, the combined analysis of the XRD and Raman results confirmed that Zn^{2+} ions occupied the available sites of Ti atoms in the anatase crystal lattice.

3.2. Electrical Response

The electrical response of *TW - Zn MOHN* to RH variations was investigated by electrical impedance spectroscopy. The *MOHN* electrical response to moisture depends on the moisture concentration and is the consequence of chemisorption and physisorption of water molecules along the surface, and on the porous structure of these nanostructures.

For low moisture concentrations, only chemisorption takes place; this occurs when the first layer of water molecules that will cover the oxides surface and porous structure gets formed. This layer, which is strongly bonded to the oxides, covers entirely the contact surface (including the open porous surface) of the materials at around 30 to 40% RH concentration. At this point, oxygen from the humidified air at room temperature

is typically adsorbed in the form of O^- , O^{2-} , O_2^- and O_2^{2-} ions. As RH concentration keeps increasing, a first physisorbed layer forms on top of the chemisorbed one: with continuous increment of moisture concentration, subsequent physisorbed layers form one after the other. However, all physisorbed layers are unstable and can be easily removed by increasing the temperature or by decreasing RH [7,30]. At this stage, H_3O^+ ions with a high quantity of H^+ protons, get formed and start participating as charge carriers, a process known as Grotthuss mechanism [31]. Once the hydronium chemical bonds are instable, H^+ protons hopping to the nearest water molecule takes place; consequently, H_2O molecules get ionized and form H_3O^+ ions, which perpetuate the charge transportation, unless, the material is heated or the RH concentration is reduced.

As the amount of water molecules begins to get saturated over the materials surface, they start to condense in the existing pore structure, within the bulk of the sensor material. When the pores in the mesoporous region (pores around 10–100 nm) get totally filled with water, new carrier paths are established for ions migration.

The measured impedance spectra highlight the different phenomena of electrical conduction and polarization that occur in these materials in the presence of water molecules, making the use of electrical impedance spectroscopy a very powerful technique in the evaluation of the materials future use in sensing devices.

In Figure 6 are plotted the Nyquist plots of TW , $TW - Zn2$, and $TW - Zn4$, in the full range of relative humidity (10–100% RH).

With the increase in RH concentration, a maximum value in impedance is observed for all tested samples. From Figure 6 this characteristic is perceived in the Nyquist plots (imaginary *versus* real parts of the impedance, $-\text{Im } Z \times \text{Re } Z$) for all samples. This type of behavior is a typical of a p-to n-type conduction transition in materials [32–35].

Although this phenomenon has already been reported in gas sensing metal oxide based devices, the mechanism that governs this transition has not been widely described in the literature. For RH sensing with high surface area *MOHN* (produced by the suggested preparation route), at low RH regime, the oxygen ions from ambient air and moisture molecules act as different agents when adsorbed on the material surface, with direct influence on the conduction properties. Herein, at low RH concentrations, oxygen from the humidified air at room temperature (in the form of O^- , O^{2-} , O_2^- and O_2^{2-} ions) are preferentially adsorbed on the surface of *MOHN* films, by capturing electrons from the conduction band [35].

This process results in the formation of an electron depletion layer [32,35], which causes the decrease in the density of free electrons and their entrapment by holes in the valence band. Consequently, the impedance of the material increases due to the removal of charge carriers from the conduction band. With the beginning of exposure to moisture, the surface of the material also begins to adsorb oxygen from the water molecules, but at a much lower rate than that of ambient oxygen, which does not favor their interaction. At this point, it is suggested that there are no significant surface active sites available for H_2O gas adsorption. Thus, the increase in system resistance is attributed to the occupying of negatively charged surface of oxygen from the air instead of moisture ions. With increasing RH, moisture adsorption tends to occur primarily by replacing the initially adsorbed oxygen ions.

When the *MOHN* is exposed to increasing RH concentrations in a low range (up to 40% of RH), the water vapor ions will progressively substitute the oxygen from the air and promote the distribution of surface adsorbed active sites. At this stage, the distance between ions from both oxygen sources will become smaller, with a consequent increase in the chemical interaction between them on the materials surface.

At this stage, water adsorption can be favoured if the sensing materials possess high surface area to volume ratio. It is known that adsorption of water vapour on the materials surface is promoted by a higher contact surface area, due to its porous nature, which affects the electrical conduction; this change encompasses the resistance, capacitance or electrolytic conduction depending on the sensor type [36].

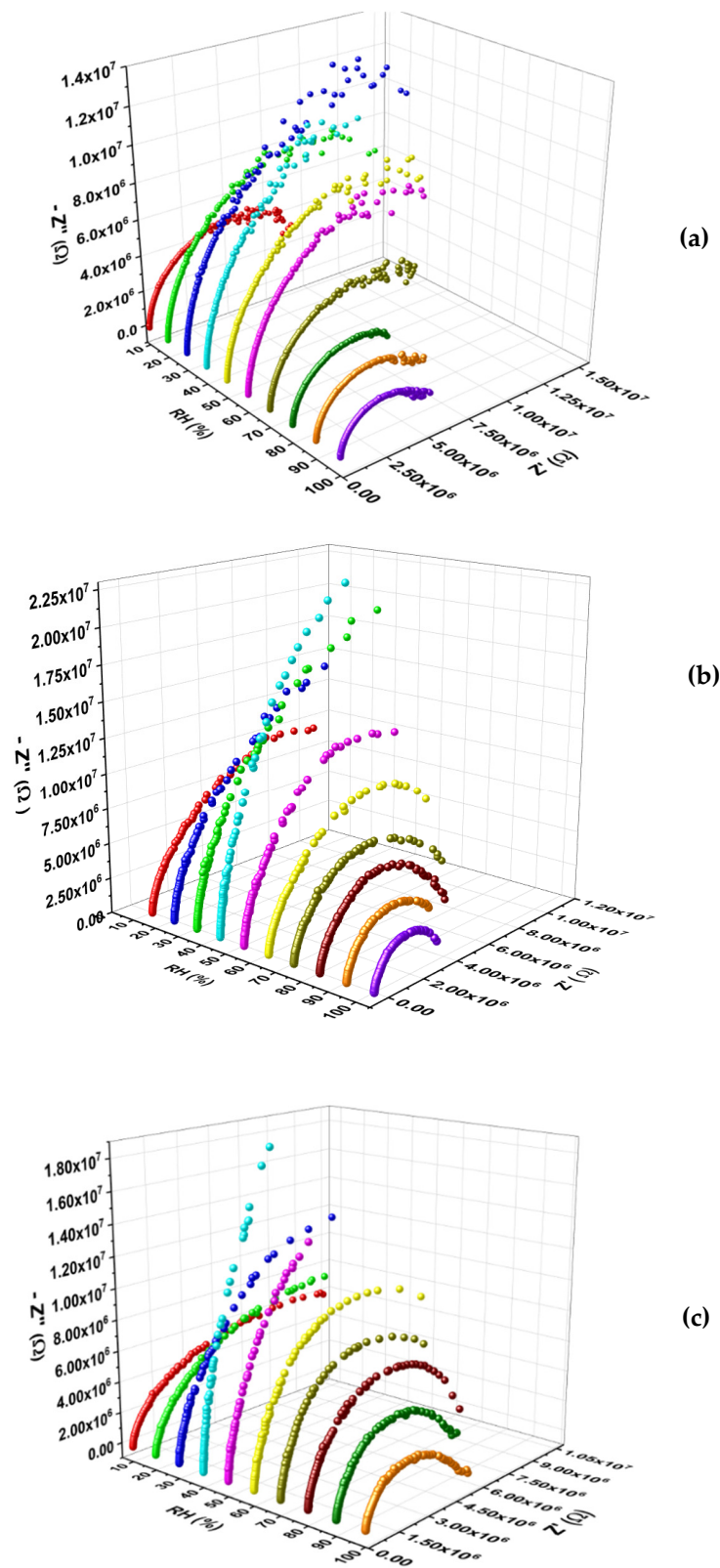


Figure 6. Nyquist Plot of the MOHN obtained samples as a function of RH, in the frequency range from 400 Hz to 40 MHz, for the (a) TW, (b) TW – Zn₂, and (c) TW – Zn₄.

Adsorption of ions from moisture becomes dominant above 30–40% RH in the tested MOHN, allowing the electrons to return to the conduction band and thus defining the transition from p- to n-type conduction in these materials.

In fact, when *MOHN* is known to adsorb a large amount of oxygen from the environment at a low RH range, a significant water vapor concentration is required so that the expected usual n-type conduction process can be established (as noted for pristine anatase titanium dioxide). In sequence, when RH concentration keeps raising above 40%, the Grotthuss chain reaction dominates and ion hopping becomes the main conduction process.

As a consequence, electrons continue to be released to the conduction band, and consequently the sensors conductance increases (n-type behavior). In general, the equilibrium between these reactions defines the dominant behavior of sensing mechanism at the level of electronic bands.

The impedance of these systems continues to decrease progressively with the continuous increase of the moisture concentration, with the formation of the first and following physisorbed layers, mainly due to transport and electrical polarization mechanisms, especially the hopping conduction of protons described earlier.

As already seen in a previous work by the authors [11], the production of *MOHN* sensing films by electrospinning may allow the obtention of nanostructured systems with high surface area to volume ratio. On close inspection of the micrographs, that seems to be the case, by a regular distribution of small spherical grains with low agglomeration, contributing to a higher contact surface area. Nevertheless, the larger presence of agglomerates in samples with higher zinc content is most likely the key factor that determines their lower sensitivity, when compared to samples with 2 wt% Zn content. This further confirms the validity of electrospinning as an efficient and low-cost fabrication process compared to other approaches, such as vapor deposition, or sputtering techniques, among others.

By looking again to the Nyquist plots for all *MOHN* nanostructures, the presence of compressed semicircles indicates that conduction in these materials is dominated by relaxation processes at the surface of grains and through grain boundaries [37]. Diffusion processes are present, at least at the interface between the measuring electrodes and the material and inside the pores that get filled with water vapour. However, their diffusion contributions are clearly small with respect to the overall measured impedance of the sensors, and in comparison to the remaining conduction contributions present [12,38]. Despite the SEM images showing that the samples are highly porous, there is low evidence for the existence of a significant amount of pores in the mesoporous region (pore size ranging from units to tens of nm). This behavior is directly associated with the arrangement of nanoparticles as films on the electrodes instead of the use of volumetric pellets, in which the impedance variation has a significant influence of micro/nanopores presence [12,38]. As an example, TiO₂/WO₃ pellets (with 100/36 Titanium/tungsten atoms proportion and sintered at 600 °C) showed a typical n-type conduction behavior in the range of 0 to 100% RH, with strong influence of diffusion processes and, consequently, an impedance variation around 2 order of magnitude [38].

The TiO₂:WO₃ volumetric systems (1:1 in mol) have been also doped with 7 wt% of ZnO [12]. The results showed that the doped samples electrically respond to RH (with a n-type conduction) but with a smaller impedance variation (close to 1 order of magnitude) [12]. The transition from p- to n-type conduction has also been reported in the TiO₂:WO₃ pelletized system (1:1 in mol), induced by vanadium ions doping [27]. The dopant introduction improved the stability of the anatase phase and considerably increased the sensitivity of the final material (relative to the initial binary mixture).

Electrospun TiO₂:WO₃ models [11] were also tested as moisture sensors, with the same binary mixture proportion as that used in other previous works [12,27] and sintered at 500 °C. The p- to n-type transition was observed and related to the change in the preparation route of the sensors by electrospinning. These systems showed excellent sensitivity to RH variations (around 1 order of magnitude) compared to pelletized samples, but using a much smaller amount of sensor material.

This configuration promotes the use of a small amount of sensor material (2.24 ± 0.21 mg ($n = 3$), 2.18 ± 0.33 mg ($n = 3$) and 2.20 ± 0.29 mg ($n = 3$), from 0 to 4 wt% ZnO, respectively). The *MOHN* mass is invariant from one sample to another, with uniform distribution of the

material over the electrode area. This is a result of the proper control of the electrospinning process parameters, the use of electrospinning as part of the material preparation and the sintering process. Thus, the errors related to the impedance measurements of the samples allocated in the humidity chamber (with ambient RH stabilized before each measurement), given a *MOHN* composition, are shown negligible and the best sensitivity results can be discussed based on the material properties.

On the other hand, in this work, the sensitivity of the produced films was increased in relation to that detected in the volumetric and electrospun $\text{TiO}_2:\text{WO}_3$ models [11,38]. The obtained impedance variations greater than 1 order of magnitude are an indication that the transport and electrical polarization mechanisms, especially the hopping conduction of protons, were considerably improved by: (i) the Zn ions doping and; (ii) high surface area to volume ratio of *MOHN* promoted by the preparing alternative method of the sensor materials. Figure 7 shows the variations in the impedance modulus obtained for the *TW* and *TW – Zn* systems as a function of RH, in the 10–100% RH range.

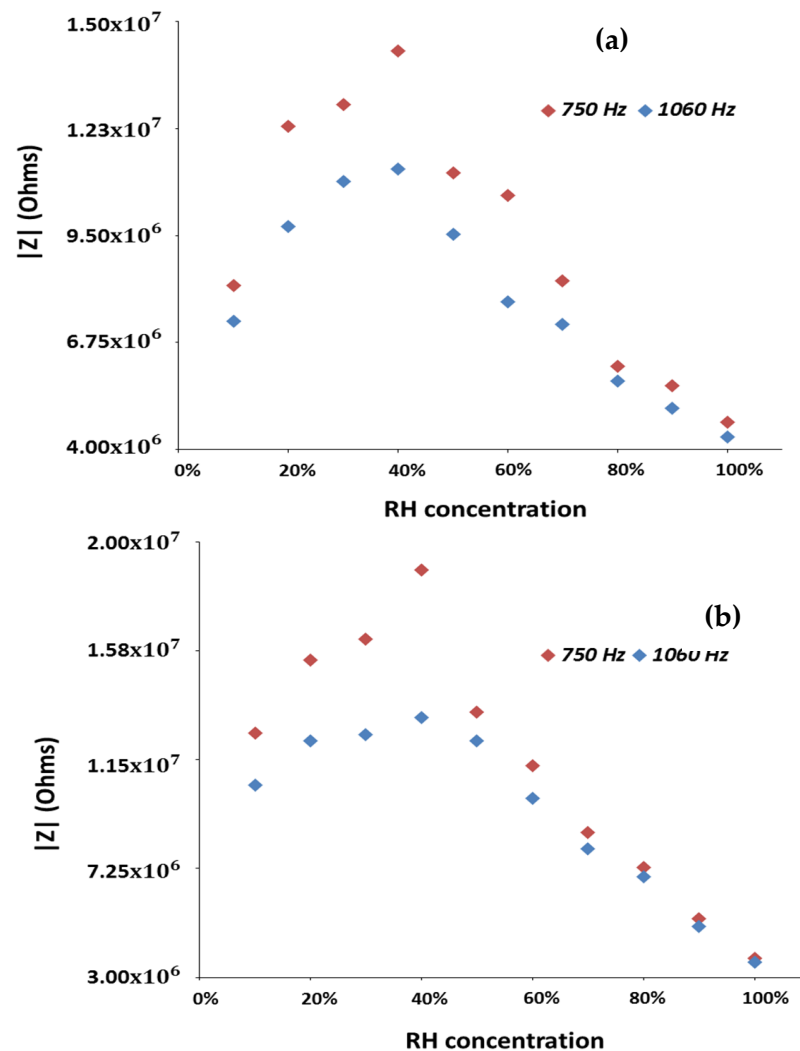


Figure 7. Cont.

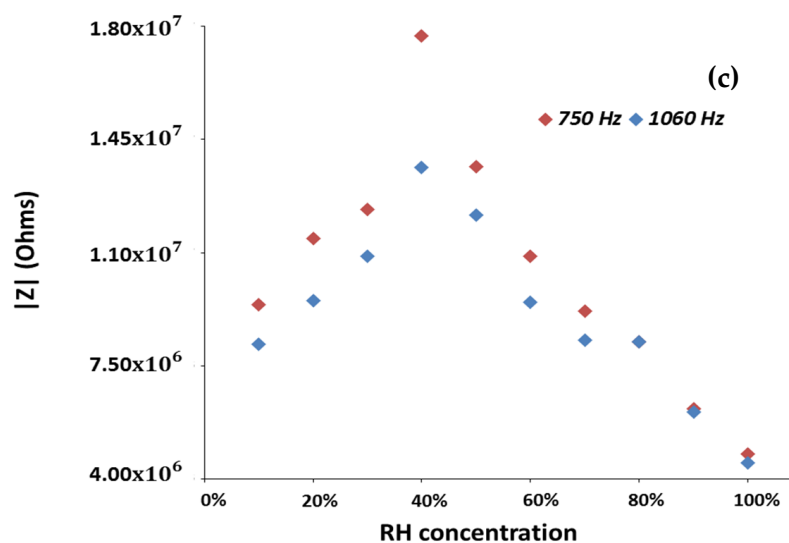


Figure 7. (a) Impedance modulus plots of the *MOHN* obtained samples as a function of RH, at two different operating frequencies, for the (a) *TW*, (b) *TW – Zn2*, and (c) *TW – Zn4*.

Frequencies above 1 kHz were also analyzed but the overall observed impedance variations were smaller than the ones here reported and plotted. The *TW*, *TW – Zn2*, and *–Zn4* samples display an overall impedance variation of 0.95, 1.52 and 1.29 order of magnitude, respectively, at the frequency of 750 Hz, where all tested sensors display the highest variations to RH changes.

These results allow to state that the use of zinc as dopant is an effective approach to improve the sensitivity of electrospun TiO_2/WO_3 *MOHN*. In fact, the *MOHN* systems containing zinc exhibit higher overall impedance to RH variations (higher overall impedance modulus variation) than those obtained with the *TW* systems (produced in the form of pellets or prepared by electrospinning, without addition of dopants) [11]. Besides, the depicted results also allow to clearly observe the mentioned p- to n-type transition, and to notice that the *MOHN* system with 2 wt% zinc content presents the highest sensitivity to moisture. Additionally, and for all sensors, it is possible to see that the frequency at which the higher overall impedance modulus variation is observable, is of 750 Hz.

In Figure 8, a close comparison of the impedance modulus variation between the three *MOHN*, done for the two test frequencies, allows to: (i) confirm that the best testing frequency is 750 Hz (the overall impedance modulus variation found at 1060 Hz is clearly smaller than the observed at 750 Hz); (ii) confirm that the system containing 2 wt% of zinc does not only exhibit always a higher overall impedance variation to moisture changes, but it also exhibits an almost linear variation with it.

The electrical response stability to moisture of *TW* and *TW – Zn* samples was tested at three RH working values (at 50, 70 and 90% RH—after the p-n transition) at 750 Hz, in terms of the relative variation of impedance, over the seven-day measurement interval under constant RH regime. Table 2 reports the stability of the electrical response based on the working values Z_i and Z_f of $|Z|$ measured after the p-n transition, and at 100% of relative humidity, respectively. The results showed that all doped samples have small variation in the measured impedance modulus values (2 – 4%) with time, considering a fixed RH (similar to the variation observed for the undoped one), with high potential usage in moisture sensing devices. The actual obtained materials, and in particular the composition doped with 2 wt% of zinc exhibits, specifically in the high humidity range, does not only show better sensitivity, but also a linear variation of the impedance modulus, characteristics not found in other materials reported in literature [39–42].

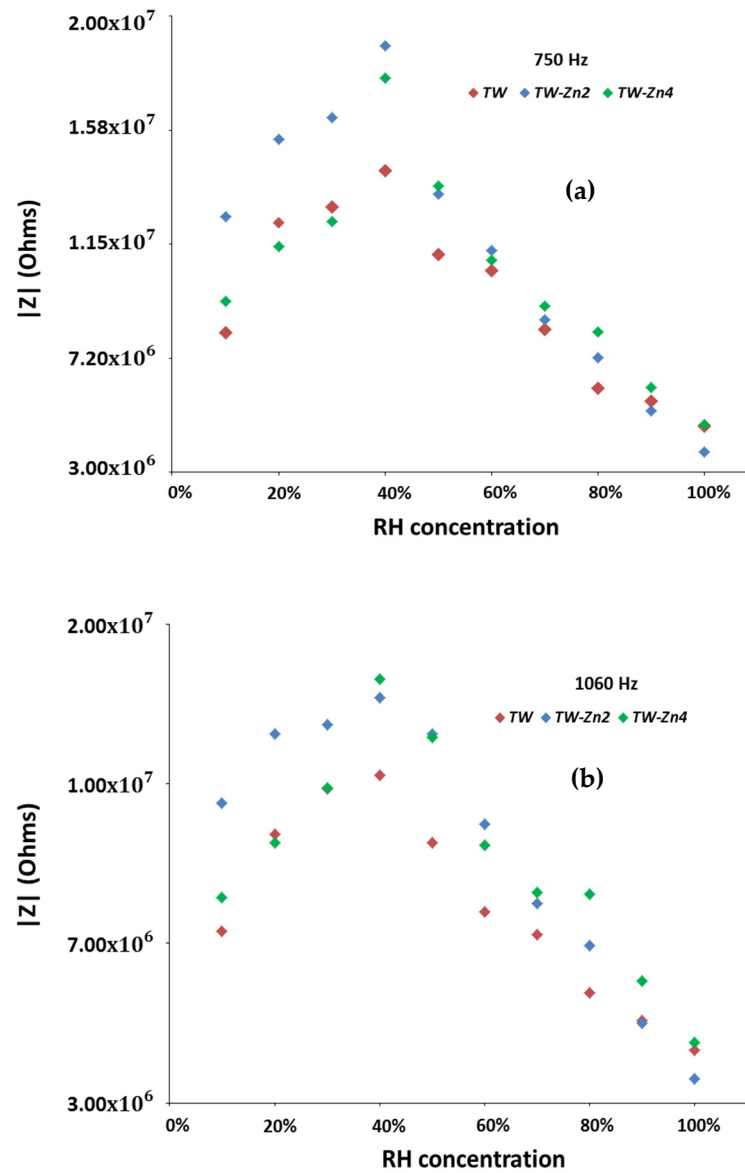


Figure 8. (a) Impedance modulus plots comparison of the MOHN obtained samples as a function of RH, at the two selected operating frequencies: (a) 750 Hz; (b) 1060 Hz.

Table 2. Electrical response stability to moisture (at 50, 70 and 90% RH) for the TW and TW – Zn MOHN produced with 2 and 4 wt% of ZnO, respectively. Similarly to the way exactitude is estimated in percentage, the sensing materials electrical response stability is estimated by the formulation indicated in Table 2.

RH (%)	TW		ZnO (wt%)	
			2	4
	Electrical response stability $(100 - \frac{Z_i - Z_t}{Z_i})$ (%)			
50	96.32	96.09	96.09	95.83
70	96.43	96.12	96.12	96.29
90	97.40	97.22	97.22	96.31

In resume, the electrical moisture sensitivity results obtained with the use of a dopant (see Figure 8 and Table 2), confirm that electrospinning is an effective and convenient processing route to prepare RH sensing devices.

4. Conclusions

Zinc-doped TiO₂:WO₃ samples were successfully prepared by electrospinning followed by sintering. The obtained electrical response to RH changes proves that electrospinning is a powerful and inexpensive technique to obtain nanostructures of mixed metal oxides for potential use in moisture sensing devices.

Besides, the present results also showed that doping is a highly valuable path that can be used to improve MOHN moisture electrical response. The microstructural characterization supports the discussion of the observed electrical response to moisture variations, obtained for the zinc-doped samples.

The highest impedance variation was obtained in sample doped with 2 wt% of zinc, which showed an overall impedance variation of more than 1 order of magnitude, with a linear electrical response. The research with these potential materials as gas sensors will be continued with the evaluation of other important parameters such as hysteresis and response and recovery time.

Author Contributions: Sample preparation and characterization, writing, editing and review, G.M.G.S., V.N.S.L., M.F.G.P., P.M.F., and E.S.A. All authors have read and agreed to the published version of the manuscript.

Funding: This research was funded by Conselho Nacional de Desenvolvimento Científico e Tecnológico (CNPq, Project 202451/2015-1) and Fundação de Amparo à Pesquisa do Estado da Bahia (FAPESB, Project 1252/2018) Brazilian research agencies. This research was also sponsored by national funds through FCT—Fundação para a Ciência e a Tecnologia, under the Project UIDB/00285/2020.

Institutional Review Board Statement: Not applicable.

Informed Consent Statement: Not applicable.

Conflicts of Interest: The authors declare no conflict of interest.

References

1. Farahani, H.; Wagiran, R.; Hamidon, M.N. Humidity sensors principle, mechanism, and fabrication technologies: A comprehensive review. *Sensors* **2014**, *14*, 7881–7939. [[CrossRef](#)]
2. Moraes, R.M.; Klem, M.D.S.; Nogueira, G.L.; Gomes, T.C.; Alves, N. Low Cost Humidity Sensor Based on PANI/PEDOT:PSS Printed on Paper. *IEEE Sens. J.* **2018**, *18*, 2647–2651. [[CrossRef](#)]
3. Tulliani, J.-M.; Inserra, B.; Ziegler, D. Carbon-Based Materials for Humidity Sensing: A Short Review. *Micromachines* **2019**, *10*, 232. [[CrossRef](#)]
4. McGhee, J.R.; Sagu, J.S.; Southee, D.J.; Evans, P.S.A.; Wijayantha, K.G.U. Printed, Fully Metal Oxide, Capacitive Humidity Sensors Using Conductive Indium Tin Oxide Inks. *ACS Appl. Electron. Mater.* **2020**, *2*, 3593–3600. [[CrossRef](#)]
5. Zhu, Z.; Lin, W.-D.; Lin, Z.-Y.; Chuang, M.-H.; Wu, R.-J.; Chavali, M. Conductive Polymer (Graphene/PPy)–BiPO₄ Composite Applications in Humidity Sensors. *Polymers* **2021**, *13*, 2013. [[CrossRef](#)]
6. Ashok, C.; Venkateswara, R.K.; Shilpa, C.C. Comparison of Metal Oxide Nanomaterials: Humidity Sensor Applications. In *Materials, Energy and Environment Engineering*; Mohan, B.R., Srinikethan, G., Meikap, B., Eds.; Springer: Singapore, 2017; pp. 267–275. [[CrossRef](#)]
7. Cappelli, I.; Fort, A.; Lo Grasso, A.; Panzardi, E.; Mugnaini, M.; Vignoli, V. RH Sensing by Means of TiO₂ Nanoparticles: A Comparison among Different Sensing Techniques Based on Modeling and Chemical/Physical Interpretation. *Chemosensors* **2020**, *8*, 89. [[CrossRef](#)]
8. Silva, G.M.G.; Leão, V.N.S.; Pereira, M.F.G.; Faia, P.M.; Araújo, E.S. Effect of Nb⁵⁺ and In³⁺ Ions on Moisture Sensitivity of Electrospun Titanium/Tungsten Oxide Nanostructures: Microstructural Characterization and Electrical Response. *Processes* **2021**, *9*, 1336. [[CrossRef](#)]
9. Zanetti, S.M.; Rocha, K.O.; Rodrigues, J.A.J.; Longo, E. Soft-chemical synthesis, characterization and humidity sensing behavior of WO₃/TiO₂ nanopowders. *Sens. Actuators B Chem.* **2014**, *190*, 40–47. [[CrossRef](#)]
10. Faia, P.M.; Libardi, J. Response to humidity of TiO₂:WO₃ sensors doped with V₂O₅: Influence of fabrication route. *Sens. Actuators B Chem.* **2016**, *236*, 682–700. [[CrossRef](#)]
11. Araújo, E.S.; Leão, V.N.S. TiO₂:WO₃ heterogeneous structures prepared by electrospinning and sintering steps: Characterization and analysis of the impedance variation to humidity. *Adv. Ceram.* **2019**, *8*, 238–246. [[CrossRef](#)]
12. Faia, P.M.; Jesus, E.L.; Louro, C.S. TiO₂:WO₃ composite humidity sensors doped with ZnO and CuO investigated by impedance spectroscopy. *Sens. Actuators B Chem.* **2014**, *203*, 340–348. [[CrossRef](#)]

13. Araújo, E.S.; Libardi, J.; Faia, P.M.; Oliveira, H.P. Characterization and Electrical Response to Humidity of Sintered Polymeric Electrospun Fibers of Vanadium Oxide-(TiO₂/WO₃). *J. Electron. Mater.* **2018**, *47*, 2018. [[CrossRef](#)]
14. Faia, P.M.; Furtado, C.S. Effect of composition on electrical response to humidity of TiO₂:ZnO sensors investigated by impedance spectroscopy. *Sens. Actuators B Chem.* **2013**, *181*, 720–729. [[CrossRef](#)]
15. Thiawong, T.; Onlaor, K.; Chaithanatkun, N.; Tunhoo, B. Preparation of copper doped zinc oxide nanoparticles by precipitation process for humidity sensing device. *AIP Conf. Proc.* **2010**, 020022. [[CrossRef](#)]
16. Yawale, S.P.; Yawale, S.S.; Lamdhade, G.T. Tin oxide and zinc oxide based doped humidity sensors. *Sens. Actuators A Phys.* **2007**, *135*, 388–393. [[CrossRef](#)]
17. Peng, X.; Chu, J.; Yang, B.; Peter, F.X. Mn-doped zinc oxide nanopowders for humidity sensors. *Sens. Actuators B Chem.* **2012**, *174*, 258–262. [[CrossRef](#)]
18. Usha, K.S.; Sivakumar, R.; Sanjeeviraja, C. Optical constants and dispersion energy parameters of NiO thin films prepared by radio frequency magnetron sputtering technique. *J. Appl. Phys.* **2013**, *114*, 123501. [[CrossRef](#)]
19. Gulshan, M.; Sai, M.L.S.; Hemalatha, T.; Sri, U.J.; Ramarao, N. Formulation and development of microspheres for the treatment of familial adenomatous polyposis. *Int. J. Appl. Pharm.* **2017**, *9*, 66–72. [[CrossRef](#)]
20. Treacy, J.P.W.; Hussain, H.; Torrelles, X.; Grinter, D.C.; Cabailh, G.; Bikondoa, O.; Nicklin, C.; Selcuk, S.; Selloni, A.; Lindsay, R.; et al. Geometric structure of anatase TiO₂(101). *Phys. Rev. B* **2017**, *95*, 075416. [[CrossRef](#)]
21. Leng, X.; Pereira, J.; Strle, J.; Bollinger, A.T.; Božović, I. Epitaxial growth of high quality WO₃ thin films. *APL Mater.* **2015**, *3*, 096102. [[CrossRef](#)]
22. Schumm, M.; Koerdel, M.; Müller, S.; Ronning, C.; Dynowska, E.; Gołacki, Z.; Szuszkiewicz, W.; Geurts, J. Secondary phase segregation in heavily transition metal implanted ZnO. *J. Appl. Phys.* **2009**, *105*, 083525. [[CrossRef](#)]
23. Yu, Q.; Fu, W.; Yu, C.; Yang, H.; Wei, R.; Sui, Y.; Liu, S.; Liu, Z.; Li, M.; Wang, G.; et al. Structural, electrical and optical properties of yttrium-doped ZnO thin films prepared by sol–gel method. *J. Phys. D Appl. Phys.* **2007**, *40*, 5592. [[CrossRef](#)]
24. Lima, F.M.; Martins, F.M.; Júnior, P.H.F.M.; Almeida, A.F.L.; Freire, F.N.A. Nanostructured titanium dioxide average size from alternative analysis of Scherrer's Equation. *Matéria* **2018**, *23*, 1–9. [[CrossRef](#)]
25. Miranda, M.A.R.; Sasaki, J.M. The limit of application of the Scherrer equation. *Acta Crystallogr. Sect. A Found. Adv.* **2018**, *74*, 54–65. [[CrossRef](#)]
26. Sahoo, S.; Arora, A.K.; Sridharan, V. Raman line shapes of optical phonons of different symmetries in anatase TiO₂ nanocrystals. *J. Phys. Chem. C* **2009**, *113*, 16927–16933. [[CrossRef](#)]
27. Faia, P.M.; Libardi, J.; Louro, C.S. Effect of V₂O₅ doping on P- to N-conduction type transition of TiO₂:WO₃ composite humidity sensors. *Sens. Actuators B Chem.* **2016**, *222*, 952–964. [[CrossRef](#)]
28. Su, C.Y.; Lin, H.C.; Lin, C.K. Fabrication and optical properties of Ti-doped W₁₈O₄₉ nanorods using a modified plasma-arc gas-condensation technique. *J. Vac. Sci. Technol. B* **2009**, *27*, 2170–2174. [[CrossRef](#)]
29. Yang, C.C.; Li, S. Size-dependent Raman red shifts of semiconductor nanocrystals. *J. Phys. Chem. B* **2008**, *112*, 14193–14197. [[CrossRef](#)]
30. Raji, P.; Binitha, H.S.; Kumar, K.B. Synthesis and humidity sensing properties of Sn-doped nano-TiO₂. *J. Nanotechnol.* **2011**, *2011*, 569036. [[CrossRef](#)]
31. Agmon, N. The Grotthuss mechanism. *Chem. Phys. Lett.* **1995**, *244*, 456–462. [[CrossRef](#)]
32. Gurlo, A.; Bârsan, N.; Oprea, A.; Sahm, M.; Sahm, T.; Weimar, U. An n-to p-type conductivity transition induced by oxygen adsorption on α -Fe₂O₃. *Appl. Phys. Lett.* **2004**, *85*, 2280. [[CrossRef](#)]
33. Sumets, M.; Dannangoda, G.C.; Kostyuchenko, A.; Ievlev, V.; Dybov, V.; Martirosyan, K.S. Temperature transition of p- to n-type conduction in the LiNbO₃/Nb₂O₅ polycrystalline films. *Mater. Chem. Phys.* **2017**, *191*, 35–44. [[CrossRef](#)]
34. Bohra, A.K.; Bhatt, R.; Singh, A.; Bhattacharya, S.; Basu, R.; Meshram, K.N.; Sarkar, S.K.; Bhatt, P.; Patro, P.K.; Aswal, D.K.; et al. Transition from n-to p-type conduction concomitant with enhancement of figure-of-merit in Pb doped bismuth telluride: Material to device development. *Mater. Des.* **2018**, *159*, 127–137. [[CrossRef](#)]
35. Gurlo, A.; Sahm, M.; Oprea, A.; Bârsan, N.; Weimar, U. A p-to n-transition on α -Fe₂O₃-based thick film sensors studied by conductance and work function change measurements. *Sens. Actuators B Chem.* **2004**, *102*, 291–298. [[CrossRef](#)]
36. Blank, T.A.; Eksperiandova, L.P.; Belikov, K.N. Recent trends of ceramic humidity sensors development: A review. *Sens. Actuators B Chem.* **2016**, *228*, 416–442. [[CrossRef](#)]
37. Bârsan, N.; Grigorovici, R.; Ionescu, R.; Vancu, A. Mechanism of gas detection in polycrystalline thick film SnO₂ sensors. *Thin Solid Films* **1989**, *171*, 53–63. [[CrossRef](#)]
38. Faia, P.M.; Ferreira, A.J.; Furtado, C.S. Establishing and interpreting an electrical circuit representing a TiO₂–WO₃ series of humidity thick film sensors. *Sens. Actuators B* **2009**, *140*, 128–133. [[CrossRef](#)]
39. Ghalamboran, M.; Saedi, Y. TiO₂-TiO₂ composite resistive humidity sensor: ethanol crosssensitivity. *IOP Conf. Ser. Mater. Sci. Eng.* **2016**, *108*, 012039. [[CrossRef](#)]
40. Shakya, V.; Pandey, N.K.; Misra, S.K.; Roy, A. Electrical and optical properties of ZnO–WO₃ nanocomposite and its application as a solid-state humidity sensor. *Bull. Mater. Sci.* **2017**, *40*, 253–262. [[CrossRef](#)]
41. Li, P.; Zheng, X.; Zhang, Y.; Yuan, M.; Jiang, B.; Deng, S. Humidity sensor based on electrospun (Na_{0.5}Bi_{0.5})_{0.94}TiO₃–Ba_{0.06}TiO₃ nanofibers. *Ceram. Int.* **2015**, *41*, 14251–14257. [[CrossRef](#)]
42. Sentürk, E.; Duman, S.; Bağcı, S.; Soykan, H.S.; Aslanoglu, Z. Humidity sensing properties of steatite ceramic containing B₂O₃. *Sens. Actuators A Phys.* **2016**, *240*, 80–84. [[CrossRef](#)]